Numerical-experimental Method for the Analysis of Residual Stresses in Cold-expanded Holes

B. Zuccarello & G. Di Franco

Experimental Mechanics
An International Journal

ISSN 0014-4851

Exp Mech
DOI 10.1007/s11340-012-9669-2

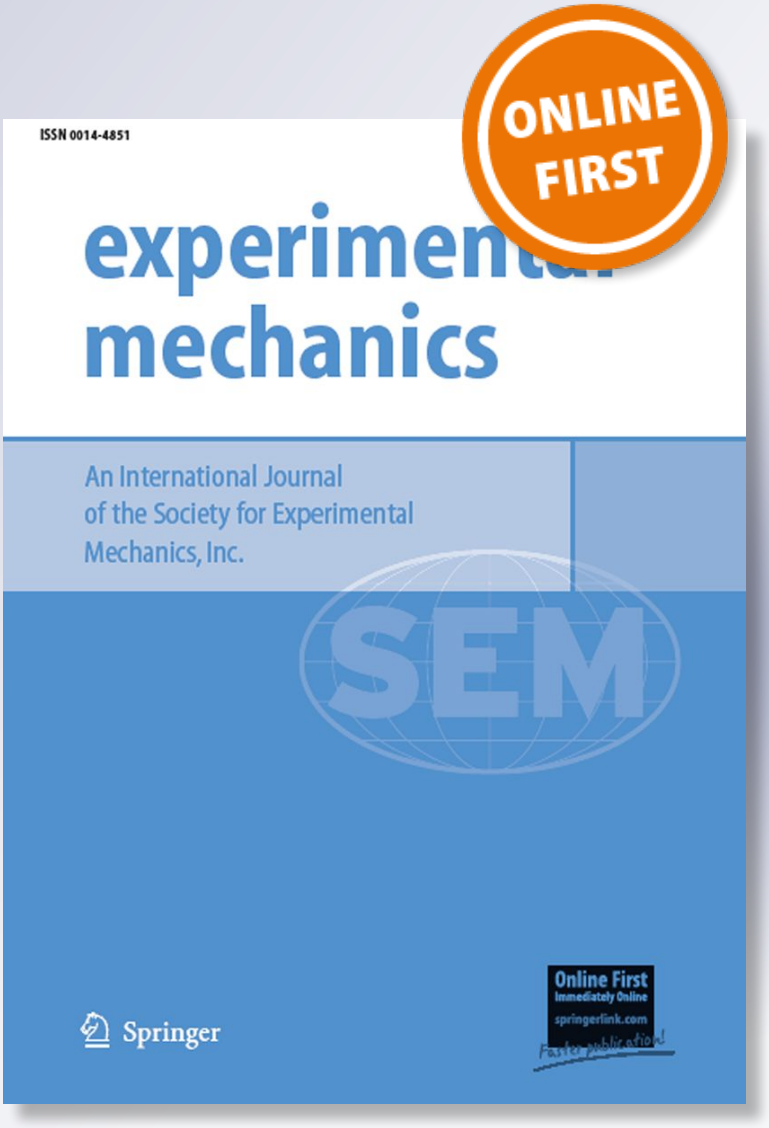

Springer

Experimental Mechanics
DOI 10.1007/s11340-012-9669-2

Numerical-experimental Method for the Analysis of Residual Stresses in Cold-expanded Holes

B. Zuccarello · G. Di Franco

Received: 22 December 2011 / Accepted: 14 August 2012

Abstract Hole cold expansion is a technique widely used to improve the fatigue life of components with holes, e.g. bolted or riveted joints. As it has been demonstrated in literature by analytical, numerical and experimental analyses carried out by several authors, the compressive residual stresses introduced by the hole cold expansion have a beneficial influence on both the static and the fatigue strength of the treated component, because they reduce significantly the typical stress peaks around the hole due to stress concentration. In the literature, various analyses of the residual stresses introduced by the hole cold expansion have been performed by using several methods such as X-ray diffraction, neutron diffraction and the modified Sachs method. Unfortunately, all these method are affected by some limitations: low measurement depth (X-ray method), complex measurement procedure (neutron diffraction method) and approximate formulation (Sachs method). In order to overcome such drawbacks, in this study a new mechanical method, based on an innovative extension of the "rectilinear groove method" associated with the classical "integral method" calculation procedure, is proposed. Experimental assessment of the proposed method has been performed by using aluminum 5083 H321 specimens with holes subjected to various levels of cold expansion.

Keywords Residual stresses · Hole cold expansion · Mechanical methods · Fatigue strength

B. Zuccarello (✉) · G. Di Franco
Dipartimento di Ingegneria Chimica, Gestionale, Informatica, Meccanica, University of Palermo,
Viale delle Scienze,
90128 Palermo, Italy
e-mail: bernardo.zuccarello@unipa.it

Introduction

In the past years the modern aeronautical industry has developed lighter aircrafts characterised by both better performances and significant reduction of fuel consumption and maintenance costs. Taking into account that fatigue failure is typical of such components, various modern techniques are implemented to improve the fatigue endurance. Among them, the most common one is the so called *hole cold expansion* (HCE) [1, 2]. This technique is applied to components with holes, such as aluminum panels that are usually connected to the primary structure with bolted or riveted joints. In the HCE the introduction of significant circumferential compressive residual stresses (RS) around the hole as well as the decreasing of surface roughness produced by the tool forcing, lead to a significant increasing of the fatigue life of both new structural components and in service structural components.

In general the HCE consists of forcing a conical-cylindrical pin in the hole to deform plastically the material around it. After the tool removal, the spring back of the material determines an axisymmetric residual stress state characterized by circumferential residual stresses (RS) that are negative in the plasticized zone near the hole boundary and positive in the elastic zone far from the hole boundary. Radial stresses, instead, are negligible near the hole edge so that they do not influence the fatigue crack initiation and therefore the fatigue life of the component that, therefore, is mainly influenced by the state of circumferential residual stresses.

Figure 1 shows the typical circumferential residual stress (σ_c) distribution obtained by the HCE. It is seen how near the hole edge the compressive circumferential RS increase (in magnitude) with the radial distance, reaching a maximum absolute value close to the yield

Published online: 20 September 2012

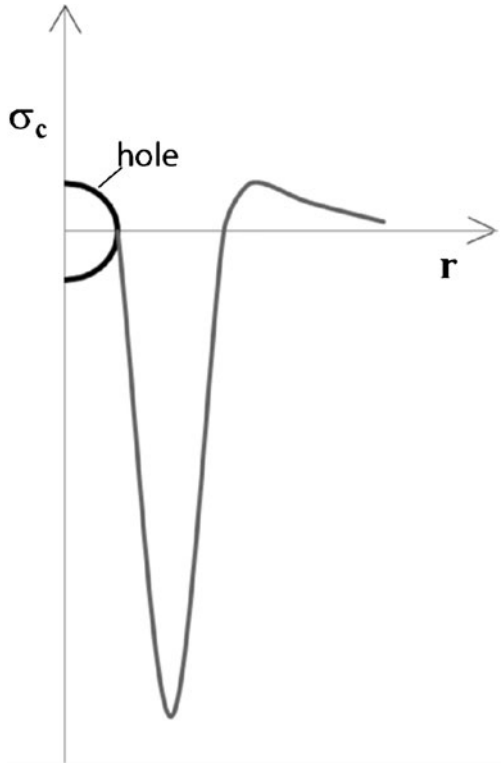

Fig. 1 Typical plot of the circumferential residual stress in cold-expanded holes

stress, than they decrease up to zero at a radial distance from the hole edge equal to about the hole diameter. In general, the RS distribution introduced by the HCE is related to the mechanical properties of the material (Young's modulus, yield stress etc.) as well as to the forcing level of pin insertion. As it is clearly demonstrated in [3, 4], the fatigue life improvement is mainly related to the circumferential compression RS that prevent the crack opening under load leading to a slower rate of the fatigue crack propagation. Detailed studies on the correlation between the HCE and the fatigue strength were carried out by several authors. In detail, Soel et al. [5] and Gopalakrishna et al. [6] have analyzed the case of elliptical pins and the case of tapered pin or a ball, respectively.

Backman et al. [7] have studied the effects of HCE by using Thermoelastic Stress Analysis (TSA) and Digital Image Correlation (DIC); by considering 2024-T3 aluminum alloy sheets they compared strains at the crack tip during crack growth around holes that had and had not been cold-expanded. Cracks originating from cold-expanded holes show lower strain values around the crack tip.

Using a numerical approach Su et al. [8] studied the effects of the application of both single and double HCE procedures, on the subsequent fatigue life of 6082-T6 aluminum alloy. Specifically, the second expansion was conducted both in the same direction (SESD) and in the opposite direction (SEOD) to the first expansion with a rigid ball. The authors found that the SEOD method can further improve the fatigue endurance of components with holes.

Compared to other techniques used to improve the fatigue strength of components with holes, the HCE has several advantages such as simplicity and low implementation costs. Moreover, it does not require additional reinforcing components that would add weight to the structures (where lightweight is a fundamental constraint in the aeronautic industry).

In order to evaluate the actual RS introduced by the HCE, it is necessary to use a reliable method of experimental RS analysis. For this purpose various techniques have been proposed in the literature.

Theoretical methods of RS analysis based on the study of analytical solutions in closed form, were developed in [9–12] by considering the case of a plate with holes subjected to an inner pressure, and to a subsequent unloading with an appropriate yield criterion.

Numerical approaches were also developed in [13–16] by using the finite element method and two-dimensional or three-dimensional approaches.

Several experimental techniques were also proposed, as the X-ray diffraction and neutron diffraction methods [17–20], as well as the modified Sachs method [12, 21]. Unfortunately, these proposed experimental methods, which should be potentially more reliable than the numerical ones, presents various drawbacks. In particular, the methods based on diffraction are strongly penalized by the limited penetration of radiation (X rays) or by the considerable overall of the method (neutron diffraction); also, the modified Sachs method is characterized by relevant theoretical approximations affecting the accuracy of the results [22].

In order to overcome these drawbacks, this paper proposes a new hybrid numerical-experimental mechanical method, based on both the machining of a through the thickness rectilinear groove obtained by successive cuts and feeds, and on the simple use of electrical resistance strain gauges (SG). The proposed method is similar to other very interesting methods recently reported in literature [23, 24], which use the Electronic Speckle Pattern Interferometry (ESPI) to obtain an accurate full-field measuring of the strains relaxed on surface when cross-slits [23] or an incremental rectilinear groove, are machined. In detail, using an original dual-axis ESPI arrangement, the cross-slitting method [23] allows the user an accurate and complete evaluation of the RS state around the intersection of two orthogonal slits; therefore it can advantageously substitute the classical incremental hole drilling method (HDM) that is characterized

by a lower stress sensitivity. The method based on the incremental groove machining [24] instead, permits to perform a two dimensions RS analysis, i.e to detect the variation of the RS with depth and along the groove axis. Unfortunately, none of the two methods are suitable for the analysis of the non-uniform RS profiles near a cold-expanded hole. In fact, the cross-slitting method considers only RS uniform along the slit axis and is not able to detect the profile of the circumferential RS along the radial direction, whereas the method based on the incremental groove machining cannot be used near a boundary of the specimen or near a hole, because it assumes that the groove length is infinite to neglect boundary condition effects and relate the RS in a particular normal section of the groove with the surface strains relaxed in the same section.

As it will be explained in the following sections, the proposed method allows the user to carry out an accurate analysis of the variation of the RS along the component thickness and consequently it permits the accurate experimental analysis of the RS actually introduced by the several HCE procedures proposed in the literature [5–8].

Proposed Method

The proposed method belongs to the mechanical methods for the RS experimental analysis [25–30], based on the introduction of a geometry variation (through layer-removal, hole drilling, groove milling or similar procedures) on the component followed by the successive measurement of the strains relaxed on the surface.

In detail, the proposed method allows the user to analyze the distribution of the circumferential RS of a generic component with holes, by milling with three successive cuts (see Fig. 2) a through the thickness groove along the radial direction. Each cut is carried out by n subsequent radial feeds, from the edge of the hole until a maximum groove radial length. The strains relaxed at the surface after each radial feed, are measured by using two electrical SGs installed on both the opposite surfaces of the component whose axes are aligned with the circumferential direction. The proposed method consists of the following successive steps:

1. installing two circumferential SGs (SG 1 and SG 2) on the two opposite surfaces of the component, near the hole and properly positioned to enable the successive milling of the rectilinear radial grooves (see Fig. 2(a));
2. milling a first blind radial groove (called groove 1) on the upper surface of the analyzed component (see Fig. 2(b)), by n subsequent radial feeds until the maximum groove radial length X_{max} is reached;
3. measuring the strains relaxed in the two surfaces after each radial feed, by the two SGs;
4. milling a second blind radial groove (called groove 2) on the lower surface of the analyzed component (see Fig. 2(c)), by the same way of the first blind groove, and measuring the strains relaxed at the two surfaces after each radial feed;
5. milling the through the thickness groove by n successive feeds to remove the material placed between the two blind grooves already cut, and measuring the strains relaxed at the two surfaces after each feed. For simplicity, in the following the removal of the material placed between the two blind grooves has been indicated as "milling the groove 3" (Fig. 2(d));
6. computing the through thickness circumferential RS distribution from the surface relaxed strains measured by the two SGs.

Theoretical Analysis

The relationship between the strains relaxed at the surfaces, measured by SG 1 and SG 2 (Fig. 2) after each feed of the three grooves, and the two-dimensional distribution of the circumferential RS in the section where the grooves are milled, is obtained by an original extension of the well known Integral Method [31, 32] to the present two-dimensional case.

Specifically, by assuming an elastic residual stress relaxation, the vector $\boldsymbol{\varepsilon_{11}}$ containing the n strains measured by the SG 1 after each feed of the blind groove 1 (Fig. 2(a)), is related to the vector $\boldsymbol{\sigma_1}$ containing the corresponding mean circumferential RS σ_{1j} ($j=1...n$) in the same n radial feeds of the groove 1, by the following relationship:

$$\boldsymbol{\varepsilon_{11}} = \mathbf{A_{111}} \cdot \boldsymbol{\sigma_1}$$

where

$$\boldsymbol{\varepsilon_{11}} = \begin{bmatrix} \varepsilon_{111} \\ \varepsilon_{112} \\ \ldots\ldots \\ \varepsilon_{11n} \end{bmatrix}; \boldsymbol{\sigma_1} = \begin{bmatrix} \sigma_{11} \\ \sigma_{12} \\ \ldots\ldots \\ \sigma_{1n} \end{bmatrix}; \mathbf{A_{111}} = \begin{bmatrix} A_{1111} & & & \\ A_{1121} & A_{1122} & & \\ \ldots & \ldots & \ldots & \\ A_{11n1} & A_{11n2} & \ldots & A_{11nn} \end{bmatrix} \quad (1)$$

In equation (1) $\mathbf{A_{111}}$ is the so called "influence matrix" [22, 29], that is a lower triangular matrix of order nxn, whose elements are the so called "influence coefficients" of the Integral Method [31, 32]. Moreover, for the strain vector and the influence matrix elements the first subscript refers to the SG, the second subscript refers to the current groove, the third subscript refers to the "groove position"

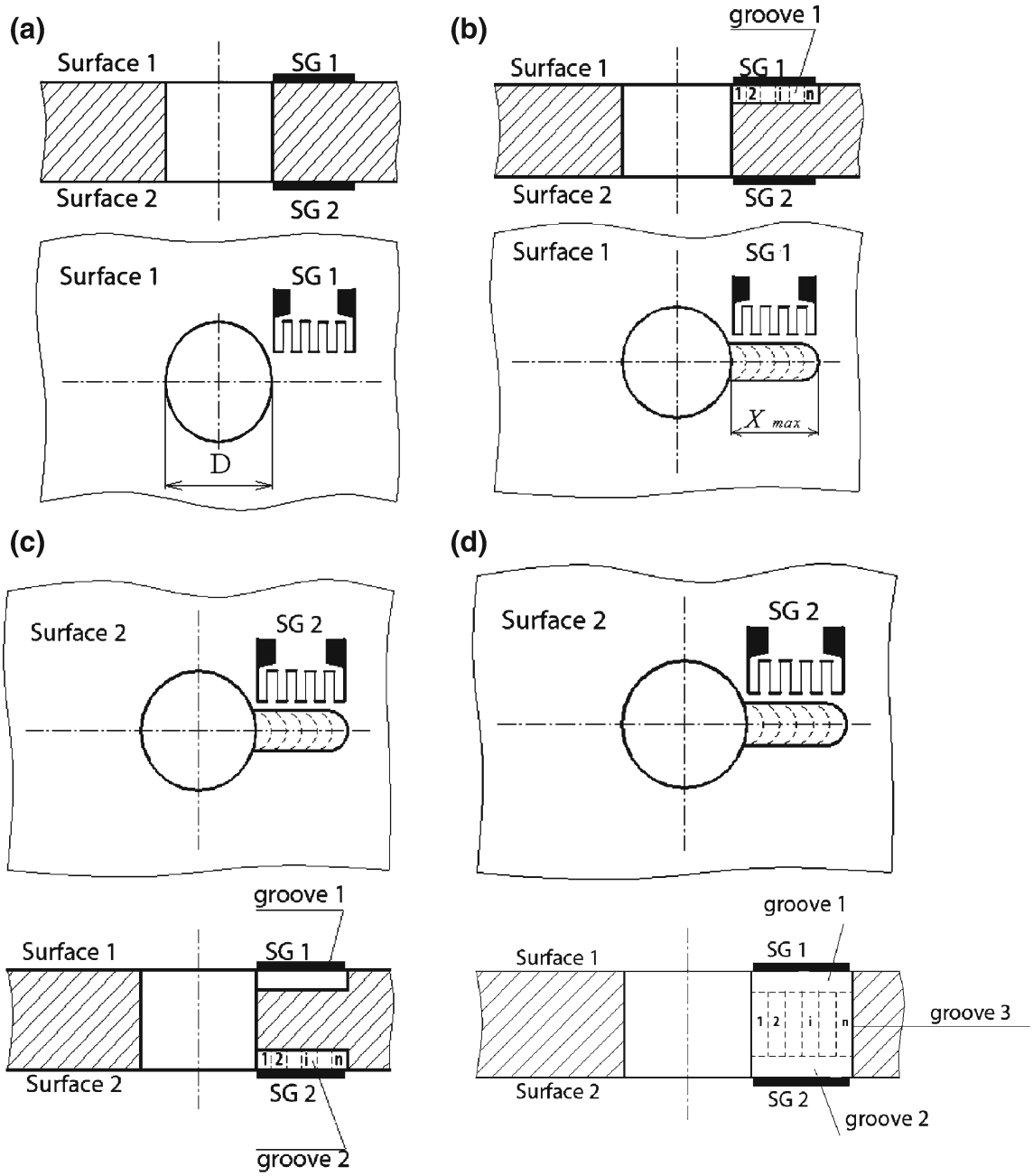

Fig. 2 The proposed method: (**a**) geometry and general notations, (**b**) execution of the groove 1 by successive feeds, (**c**) execution of the groove 2, (**d**) execution of the groove 3 by the same *n* feeds

whereas the fourth subscript refers to the "stress position". For the components of the stress vector, instead, the first subscript refers to the groove whereas the second subscript refers to the stress position.

Similarly, the vector $\boldsymbol{\varepsilon_{21}}$ of the strains measured by the SG 2 when the groove 1 is milled step by step, is related to the stress vector $\boldsymbol{\sigma_1}$ by the following equation:

$$\boldsymbol{\varepsilon_{21}} = \mathbf{A}_{211} \cdot \boldsymbol{\sigma_1}$$

where

$$\boldsymbol{\varepsilon_{21}} = \begin{bmatrix} \varepsilon_{211} \\ \varepsilon_{212} \\ \ldots\ldots \\ \varepsilon_{21n} \end{bmatrix}; \mathbf{A}_{211} = \begin{bmatrix} A_{2111} & & & \\ A_{2121} & A_{2122} & & \\ \ldots & \ldots & \ldots & \\ A_{21n1} & A_{21n2} & \ldots & A_{21nn} \end{bmatrix} \quad (2)$$

In equation (2) $\mathbf{A_{211}}$ is a lower triangular matrix of order *nxn*, similarly to matrix $\mathbf{A_{111}}$. Also in equation (2) and in all the successive equations the subscripts are identified by the same rules above outlined for equation (1).

Moreover, the strain vector $\boldsymbol{\varepsilon_{22}}$, measured through the SG 2 when the groove 2 is milled step by step, is related to the stress vector $\boldsymbol{\sigma_1}$ as well as to the stress vector $\boldsymbol{\sigma_2}$ containing the mean circumferential RS in the n feeds of the groove 2, by the following equation:

$$\boldsymbol{\varepsilon_{22}} = \mathbf{A}_{221} \cdot \boldsymbol{\sigma_1} + \mathbf{A}_{222} \cdot \boldsymbol{\sigma_2}$$

where

$$\boldsymbol{\varepsilon_{22}} = \begin{bmatrix} \varepsilon_{221} \\ \varepsilon_{222} \\ \ldots\ldots \\ \varepsilon_{22n} \end{bmatrix}; \boldsymbol{\sigma_2} = \begin{bmatrix} \sigma_{21} \\ \sigma_{22} \\ \ldots\ldots \\ \sigma_{2n} \end{bmatrix}; \mathbf{A}_{221} = \begin{bmatrix} A_{2211} & A_{2212} & \ldots & A_{221n} \\ A_{2221} & A_{2122} & \ldots & A_{222n} \\ \ldots & \ldots & \ldots & \ldots \\ A_{22n1} & A_{21n2} & \ldots & A_{21nn} \end{bmatrix};$$

$$\mathbf{A}_{222} = \begin{bmatrix} A_{2211} & & & \\ A_{2221} & A_{2222} & & \\ \ldots & \ldots & \ldots & \\ A_{22n1} & A_{22n2} & \ldots & A_{22nn} \end{bmatrix} \tag{3}$$

In equation (3) the nxn full matrix $\mathbf{A_{221}}$ gives the strain contribution (on $\boldsymbol{\varepsilon_{22}}$) due to the further relaxation of the RS contained in the vector $\boldsymbol{\sigma_1}$ (acting on groove 1) when the groove 2 is milled, whereas the nxn lower triangular matrix $\mathbf{A_{222}}$ gives the strain contribution of the RS relaxation that occurs in the current groove 2.

Similarly, the vector $\boldsymbol{\varepsilon_{12}}$ of the strains measured by the SG 1 when groove 2 is milled, is related to the stress vectors $\boldsymbol{\sigma_1}$ and $\boldsymbol{\sigma_2}$ by the following equation:

$$\boldsymbol{\varepsilon_{12}} = \mathbf{A}_{121} \cdot \boldsymbol{\sigma_1} + \mathbf{A}_{122} \cdot \boldsymbol{\sigma_2}$$

where

$$\boldsymbol{\varepsilon_{12}} = \begin{bmatrix} \varepsilon_{121} \\ \varepsilon_{122} \\ \ldots\ldots \\ \varepsilon_{12n} \end{bmatrix}; \mathbf{A}_{121} = \begin{bmatrix} A_{1211} & A_{1212} & \ldots & A_{121n} \\ A_{1221} & A_{1222} & \ldots & A_{122n} \\ \ldots & \ldots & \ldots & \ldots \\ A_{12n1} & A_{12n2} & \ldots & A_{12nn} \end{bmatrix}; \tag{4}$$

$$\mathbf{A}_{122} = \begin{bmatrix} A_{1211} & & & \\ A_{1221} & A_{1222} & & \\ \ldots & \ldots & \ldots & \\ A_{12n1} & A_{12n2} & \ldots & A_{12nn} \end{bmatrix}$$

Similarly to what said above for equation (3), in equation (4) $\mathbf{A_{121}}$ is a full matrix of order nxn, whereas $\mathbf{A_{122}}$ is a lower triangular matrix of order nxn.

Finally, the vector $\boldsymbol{\varepsilon_{13}}$ of the strains measured by SG 1 when the groove 3 is milled, is related to $\boldsymbol{\sigma_1}$ and $\boldsymbol{\sigma_2}$ as well as to the stress vector $\boldsymbol{\sigma_3}$ which contains the mean circumferential RS in the n feeds of the groove 3, by the following equation:

$$\boldsymbol{\varepsilon_{13}} = \mathbf{A}_{131} \cdot \boldsymbol{\sigma_1} + \mathbf{A}_{132} \cdot \sigma_2 + \mathbf{A}_{133} \cdot \boldsymbol{\sigma_3}$$

where

$$\boldsymbol{\varepsilon_{13}} = \begin{bmatrix} \varepsilon_{131} \\ \varepsilon_{132} \\ \ldots\ldots \\ \varepsilon_{13n} \end{bmatrix}; \sigma_3 = \begin{bmatrix} \sigma_{31} \\ \sigma_{32} \\ \ldots\ldots \\ \sigma_{3n} \end{bmatrix} \mathbf{A}_{131} = \begin{bmatrix} A_{1311} & A_{1312} & \ldots & A_{131n} \\ A_{1321} & A_{1322} & \ldots & A_{132n} \\ \ldots & \ldots & \ldots & \ldots \\ A_{13n1} & A_{13n2} & \ldots & A_{13nn} \end{bmatrix};$$

$$\mathbf{A}_{132} = \begin{bmatrix} A_{1311} & A_{1312} & \ldots & A_{131n} \\ A_{1321} & A_{1322} & \ldots & A_{1322} \\ \ldots & \ldots & \ldots & \ldots \\ A_{13n1} & A_{13n2} & \ldots & A_{13nn} \end{bmatrix}; \mathbf{A}_{133} = \begin{bmatrix} A_{1311} & & & \\ A_{1321} & A_{1322} & & \\ \ldots & \ldots & \ldots & \\ A_{13n1} & A_{13n2} & \ldots & A_{13nn} \end{bmatrix} \tag{5}$$

Similarly for the SG 2, it follows:

$$\boldsymbol{\varepsilon_{23}} = \mathbf{A}_{231} \cdot \boldsymbol{\sigma_1} + \mathbf{A}_{232} \cdot \boldsymbol{\sigma_2} + \mathbf{A}_{233} \cdot \boldsymbol{\sigma_3}$$

where

$$\boldsymbol{\varepsilon_{23}} = \begin{bmatrix} \varepsilon_{231} \\ \varepsilon_{232} \\ \ldots\ldots \\ \varepsilon_{23n} \end{bmatrix}; \mathbf{A}_{231} = \begin{bmatrix} A_{2311} & A_{2312} & \ldots & A_{231n} \\ A_{2321} & A_{2322} & \ldots & A_{232n} \\ \ldots & \ldots & \ldots & \ldots \\ A_{23n1} & A_{23n2} & \ldots & A_{23nn} \end{bmatrix};$$

$$\mathbf{A}_{232} = \begin{bmatrix} A_{2311} & A_{2312} & \ldots & A_{231n} \\ A_{2321} & A_{2322} & \ldots & A_{232n} \\ \ldots & \ldots & \ldots & \ldots \\ A_{23n1} & A_{23n2} & \ldots & A_{23nn} \end{bmatrix}; \mathbf{A}_{233} = \begin{bmatrix} A_{2311} & & & \\ A_{2321} & A_{2322} & & \\ \ldots & \ldots & \ldots & \\ A_{23n1} & A_{23n2} & \ldots & A_{23nn} \end{bmatrix} \tag{6}$$

By summing the strain vectors corresponding to the two SG when a fixed groove is milled, the following matrix relationship can be written:

$$\begin{Bmatrix} \boldsymbol{\varepsilon_{11}} + \boldsymbol{\varepsilon_{21}} \\ \boldsymbol{\varepsilon_{12}} + \boldsymbol{\varepsilon_{22}} \\ \boldsymbol{\varepsilon_{13}} + \boldsymbol{\varepsilon_{23}} \end{Bmatrix} = \begin{bmatrix} (A_{111} + A_{211}) & 0 & 0 \\ (A_{121} + A_{221}) & (A_{122} + A_{222}) & 0 \\ (A_{131} + A_{231}) & (A_{132} + A_{232}) & (A_{133} + A_{233}) \end{bmatrix} \cdot \begin{Bmatrix} \boldsymbol{\sigma_1} \\ \boldsymbol{\sigma_2} \\ \boldsymbol{\sigma_3} \end{Bmatrix} \tag{7}$$

It is noted that the super-matrix that appears into equation (7) is a lower triangular matrix of order $3n$x$3n$ and therefore it contains $3n(3n+1)/2$ non-zero influence coefficients; moreover, due to the geometric symmetry of the grooves respect to the middle plane of the examined component, it follows that:

$$\mathbf{A}_{131} = \mathbf{A}_{232}; \mathbf{A}_{231} = \mathbf{A}_{132}; \mathbf{A}_{133} = \mathbf{A}_{233} \tag{8–10}$$

From equations (8) and (9) follows that the first and the second term of the third row of the influence matrix that appears in equation (7), are equal.

Finally, denoting by $\overline{\boldsymbol{\varepsilon}}_1$, $\overline{\boldsymbol{\varepsilon}}_2$ and $\overline{\boldsymbol{\varepsilon}}_3$ the strain vectors whose components are obtained by summing the strains measured by SG 1 and SG 2 after milling of each feed of grooves 1, 2 and 3, and indicating with:

$$\begin{aligned} \mathbf{C_{11}} &= \mathbf{A_{111}} + \mathbf{A_{211}};\\ \mathbf{C_{21}} &= \mathbf{A_{121}} + \mathbf{A_{221}};\\ \mathbf{C_{22}} &= \mathbf{A_{122}} + \mathbf{A_{222}};\\ \mathbf{C_{31}} &= \mathbf{C_{32}} = \mathbf{A_{131}} + \mathbf{A_{231}};\\ \mathbf{C_{33}} &= \mathbf{2A_{133}} \end{aligned} \tag{11–15}$$

It follows that equation (7) can be written as:

$$\begin{Bmatrix} \overline{\varepsilon_1} \\ \overline{\varepsilon_2} \\ \overline{\varepsilon_3} \end{Bmatrix} = \begin{bmatrix} \mathbf{C_{11}} & 0 & 0 \\ \mathbf{C_{21}} & \mathbf{C_{22}} & 0 \\ \mathbf{C_{31}} & \mathbf{C_{31}} & \mathbf{C_{33}} \end{bmatrix} \cdot \begin{Bmatrix} \sigma_1 \\ \sigma_2 \\ \sigma_3 \end{Bmatrix} \tag{16}$$

It is to be noted that the strain components of vectors $\overline{\varepsilon_1}$, $\overline{\varepsilon_2}$ and $\overline{\varepsilon_3}$ can be obtained directly by connecting SG 1 and SG 2 on the opposite sides of the Wheatstone bridge [31] used for strains measurement. Also, the first subscript of the generic influence matrix $\boldsymbol{C_{ij}}$ refers to the groove whose milling is in progress, whereas the second subscript refers to the groove whose stress contribution is considered for the strain relaxation calculation.

Equation (16) shows that the RS in each feed of the three grooves can be calculated from the corresponding relaxed strains, by using the five influence matrices $\boldsymbol{C_{11}}$, $\boldsymbol{C_{21}}$, $\boldsymbol{C_{22}}$, $\boldsymbol{C_{31}}$ and $\boldsymbol{C_{33}}$. By using the approach already used in the Integral Method applied to the hole drilling technique [29], these matrices can be determined from the corresponding "cumulative influence functions "$\overline{C}_{11}(x_1, X_1)$, $\overline{C}_{21}(x_1, X_1)$, $\overline{C}_{22}(x_2, X_2)$, $\overline{C}_{31}(x_1, X_1)$ and $\overline{C}_{33}(x_3, X_3)$ [22, 29], in which x_j and X_j are the current radial distance from the hole edge and the radial length of the *i-th* groove, respectively; the introduction of these function permits to concentrate all the information contained in the several influences matrixes $\boldsymbol{C_{ij}}$ into simple low degree polynomials; moreover they allows the user to compute the RS profile by considering a distribution of stress positions different from the distribution of the actual radial feeds of the grooves; this permits in general to the user to choice properly the number and the distribution of the stress points to use to obtain an accurate description of the particular RS profile analyzed. The generic cumulative influence function $\overline{C}_{ij}(x_j, X_j)$ is defined by the relationship:

$$\overline{C}_{ij}(x_i, X_j) = \int_0^x \widehat{F}_{ij}(x_j, X_j)\, dx_j \quad (i,j = 1,2,3) \tag{17}$$

where $\widehat{F}_{ij}(x_j, X_j)$ is the influence function related to the groove-SGs geometry. As it is well known in the Integral Method [31, 33, 36], $\widehat{F}_{ij}(x_j, X_j)$ is the strain relaxation per unit feed caused by a unit stress at the stress position x_i when the *j-th* groove has length X_j.

For a fixed hole radius, these cumulative influence functions are defined by the following geometrical parameters (see also Fig. 3):

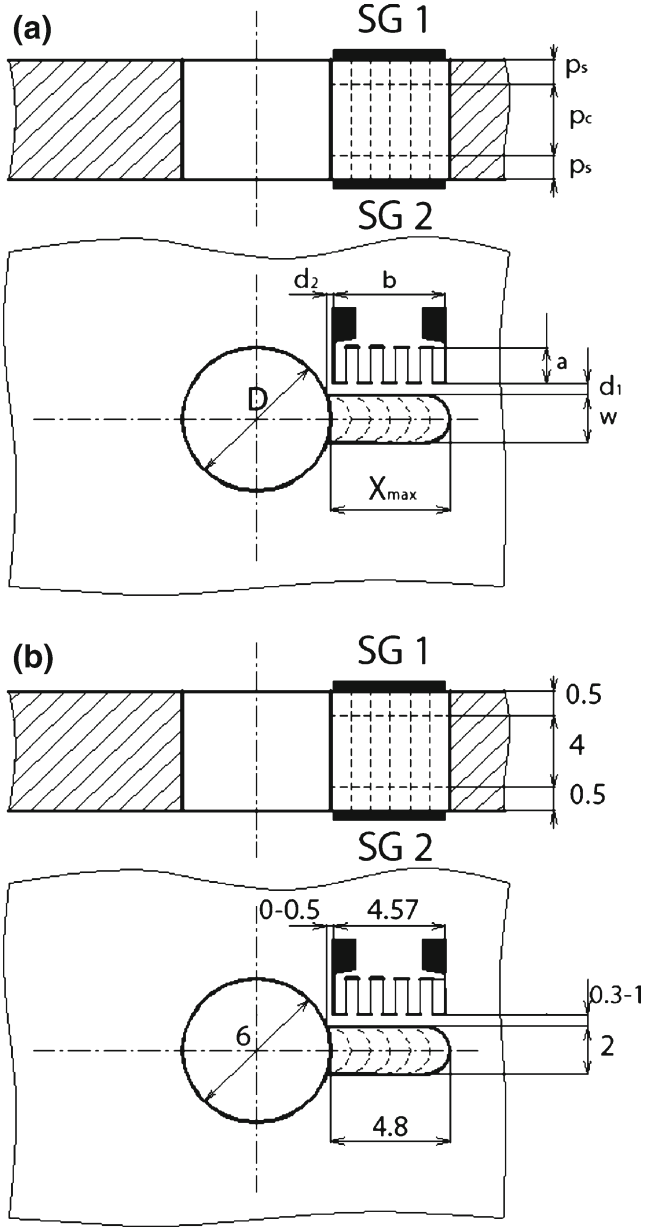

Fig. 3 Geometrical influence parameters (**a**) and optimized values adopted in the numerical simulations (**b**)

1. groove width, w;
2. depth p_s of the superficial grooves 1 and 2, and depth p_c of the central groove 3;
3. maximum radial length of the grooves, X_{max};
4. dimensions (a and b) of the SGs and their position defined by the distance d_1 from the groove edge, and the distance d_2 from the hole edge.

In particular, by taking into account the typical RS distribution produced by the HCE (see Fig. 1), the maximum radial length of the grooves, X_{max}, may be set equal to about 0.8 times the hole diameter D. Also, in order to consider as negligible the difference between the circumferential RS

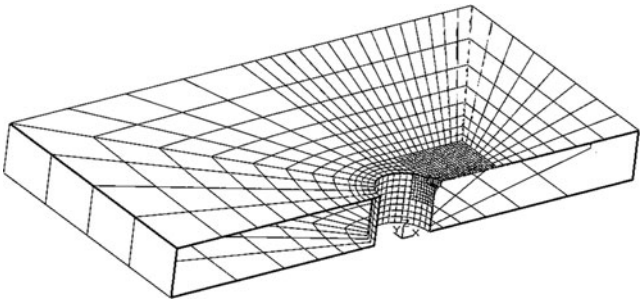

Fig. 4 BEM model corresponding to the second feed of groove 1

detected and the RS orthogonal to the groove edge, i.e. the RS totally relaxed, the groove width w must be appropriately small; from simple stress analysis it is found that the use of groove width $w \leq 0.33\ D$ ensures that such a difference is always less than 10 %.

The depth p_s of the superficial grooves 1 and 2, is to be chosen as a compromise between an accurate measurement of the corresponding superficial RS (small p_s) and a good stress relaxation sensitivity (high p_s). Preliminary numerical investigations have shown that the maximum stresses that occur on both component surfaces (input and output of the tool) can be estimate accurately by using $p_s=0.1\ s$, being s the component thickness; such a value gives in general a satisfactory sensitivity to stress relaxation. Consequently it follows that $p_c=0.8\ s$.

The sizes a and b of the SG are related to both the stress relaxation sensitivity and the maximum radial length of the grooves. To obtain high stress relaxation sensitivity, it is necessary to use SGs having b close to X_{max}, and small grid length so that the SG measurement area is very close to the maximum stress relaxation zone. Numerical simulations have shown that a sufficient stress sensitivity is obtained

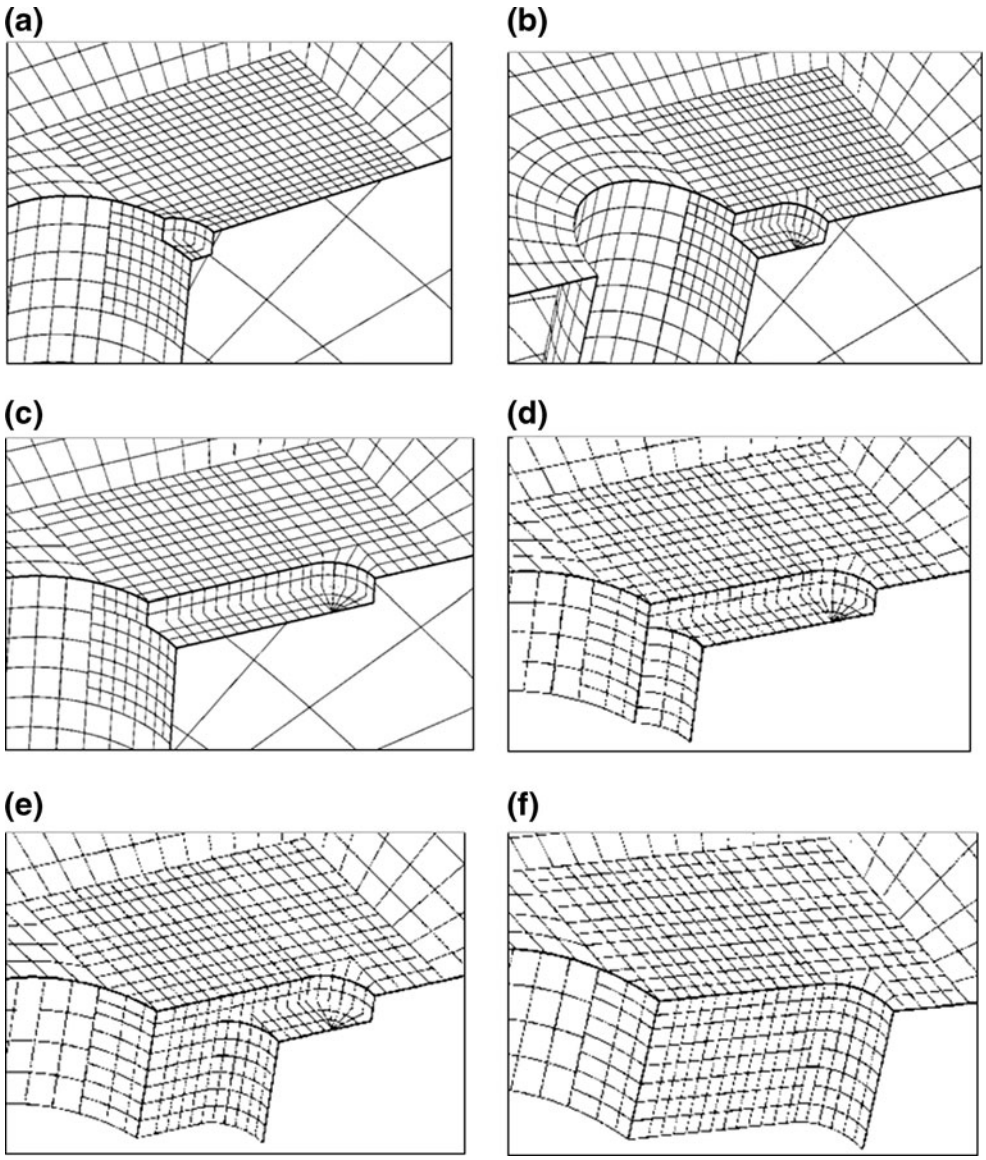

Fig. 5 Particulars of the discretization near the groove for some models: (**a**) second feed of groove1, (**b**) fourth feed of groove 1, (**c**) sixth feed of the groove 1, (**d**) second feed of the groove 3 (**e**) fourth feed of groove 3, (**f**) sixth feed of the groove 3

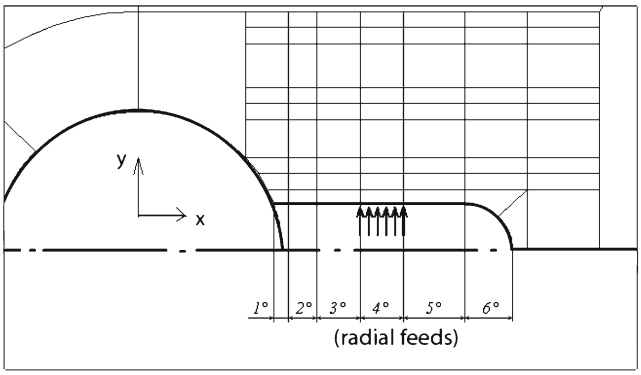

Fig. 6 Model and load case used to calculate the influence coefficients C_{1164} (fourth feed of the groove 1 when 6 feeds have been executed)

by using SG with $a \leq 7\ p_s$ although values near to 3 p_s can be considered optimal.

The SG position, defined by the distances d_1 and d_2, is essentially related to both the sensitivity to the stress relaxation and the spurious effects due to further RS introduced by the groove milling. To maximize the stress relaxation sensitivity, particularly that relative to the first feed of each groove, it is ideal to use $d_2 \approx 0$ mm. In accordance with ASTM E 837-99 [34], a satisfactory compromise between stress sensitivity and spurious effects related to plastic strain due to groove milling, is obtained by using $d_1 \approx 0.3$ mm.

Numerical Analysis

The evaluation of the cumulative influence functions has been performed by polynomial interpolation of the influence coefficients calculated by using the Boundary Elements Method (BEM) and the commercial code BEASY 9.0®. The numerical model considers a rectangular aluminum (E=70 GPa, ν=0.3) plate of 50×50×5 mm with a centered hole having diameter D=6 mm. In more detail, the geometry of the grooves-SG system simulated numerically, which is in accordance with all the considerations reported in the previous section, is shown in Fig. 3.

In order to have a satisfactory resolution of the RS curve and a limited number of feeds, n=6 radial feeds with increasing amplitudes ΔX=0.3, 0.3, 0.9, 0.9, 1.2, 1.2 mm, have been considered (total radial groove length X_{max}=4.8 mm).

The mesh of the surfaces of the BEM models, developed by preliminary convergence tests, were made by using about 1000 quadratic boundary elements (square with 9 nodes and triangular with 6 nodes). As an example, Fig. 4 shows the model that represents the groove 1 when the second feed is carried out. Figure 5 shows, the particular of the area close to the groove for different feeds.

It is to be noted that for the calculation of the $3n$ $(3n+1)/2$ influence coefficients, $3n$ different models and $3n(3n+1)/2$ load cases with unitary circumferential stress applied to a single feed, have to be considered. As an example Fig. 6 shows the model and the load case used to evaluate the C_{1164} influence coefficient (i.e the fourth coefficient of the sixth row of the matrix $\boldsymbol{C_{11}}$).

In more detail, the influence coefficients have been computed from the displacement field provided directly by the BEASY code; to this aim a special routine that implements in Matlab® [22] the simple procedure described in [35], has been used to compute the mean strain measured by the SG directly from the displacement along the top and bottom edges of the SG grid.

As an example, Fig. 7 shows the plot of some influence coefficients relative to a common SG type MM-CEA-13-060CP-120 having a grid length equal to 1.52 mm and grid width of 4.57 mm, for $0.3 \leq d_1 \leq 1$ mm and $0 \leq d_2 \leq 0.5$ mm.

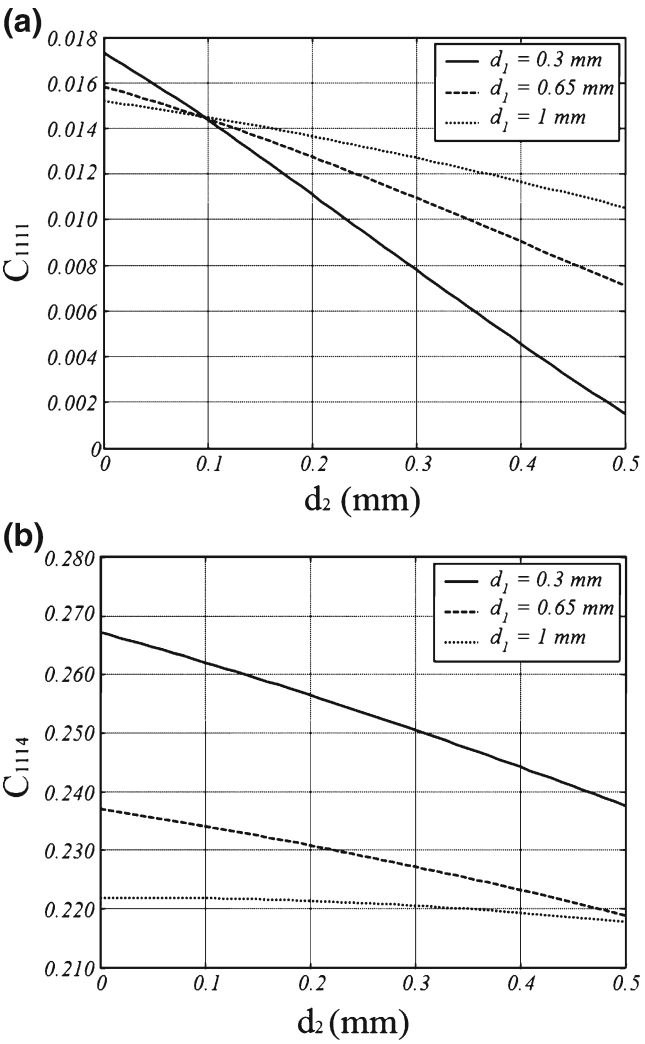

Fig. 7 Plot of some influence coefficients for SG type MM-CEA-120-13-060CP

Using the same approach commonly employed in the hole drilling method [30], from the matrix $\boldsymbol{C_{11}}$, $\boldsymbol{C_{21}}$, $\boldsymbol{C_{22}}$, $\boldsymbol{C_{31}}$ and $\boldsymbol{C_{33}}$, the corresponding cumulative influence functions $\overline{C}_{11}(x_1, X_1)$, $\overline{C}_{21}(x_1, X_1)$, $\overline{C}_{22}(x_2, X_2)$, $\overline{C}_{31}(x_1, X_1)$ e $\overline{C}_{33}(x_3, X_3)$ have been determined.

In this work in particular the cumulative influence functions have been computed by a polynomial fitting of the corresponding discrete values obtained as:

$$\left(\overline{C}_{\mathrm{ij}}\right)_{\mathrm{l,m}} = \sum_{t=1}^{m} \left(C_{\mathrm{ij}}\right)_{\mathrm{l,t}} \tag{18}$$

In equation (18) the first member term is the particular value of the cumulative influence function that refers to the *m-th* feed of the *j* groove when *l* feeds of the groove *i* have been performed; the terms of the second member are the elements of the matrixes $\boldsymbol{C_{ij}}$ that appears in equation (16).

Synthetically, the MATLAB routine calculates first the elements of each matrix $\boldsymbol{C_{ij}}$ from the BEM results, then it computes the discrete values of the matrix elements $\left(\overline{C}_{\mathrm{ij}}\right)_{\mathrm{l,m}}$ by equation (18) and, finally, it determines the functions $\overline{C}_{\mathrm{ij}}\left(x_i, X_j\right)$ by means of a polynomial fitting of $\left(\overline{C}_{\mathrm{ij}}\right)_{\mathrm{l,m}}$. The functions $\overline{C}_{\mathrm{ij}}\left(x_i, X_j\right)$ are characterized by regular patterns with low gradients, and in general the use of simple third order polynomial permits to fit the discrete values with error lower than 5 %. The so obtained polynomials that represent the five cumulative influence functions for d_1=0.3 mm and d_2=0 mm, are reported here to provide a quantitative example:

$$\overline{C}_{11}(x_1, X_1) = 10^{-2}\left(7.4375x_1 + 0.77937x_1^2 - 0.2114x_1^3 + 0.036377x_1^2X_1 + 0.10003x_1X_1^2 - 0.50528X_1 + +0.5868X_1^2 - 0.092754X_1^3\right)$$
$$\overline{C}_{12}(x_2, X_2) = 10^{-3}\left(5.1491x_2 - 0.53115x_2^2 + 6.8468e-002x_2^3 - 6.5857e-002x_2^3X_2 - 0.16111x_2X_2^2 + 1.7856X_2 - 1.4469X_2^2 + 0.21992X_2^3\right)$$
$$\overline{C}_{22}(x_2, X_2) = 0^{-2}\left(7.4325x_2 + 0.78556x_2^2 - 0.21153x_2^3 + 0.035298x_2^2X_2 + 0.10038x_2X_2^2 - 0.50023X_2 + 0.55438 \cdot X_2^2 - 0.092055X_2^3\right)$$
$$\overline{C}_{13}(x_3, X_3) = 10^{-2}\left(9.4482x_3 + 1.3136x_3^2 - 0.27947x_3^3 + 3.3585e-003x_3^2X_3 - 0.15344x_3X_3^2 + 0.10973X_3 + 0.36688X_3^2 - 0.082102X_3^3\right)$$
$$\overline{C}_{33}(x_3, X_3) = 10^{-2}\left(20.569 \cdot x_3 + 3.5039 \cdot x_3^2 - 0.92736 \cdot x_3^3 + 0.74336 \cdot x_3^2 \cdot X_3 - 0.19298 \cdot x_3 \cdot X_3^2 + 0.71492 \cdot X_3 - 0.2231 \cdot X_3^2 + 0.021982 \cdot X_3^3\right)$$

It is to be noted that the use of different fitting functions, as wavelets or spline functions could give a better fitting, i.e., a better definition of the functions $\overline{C}_{\mathrm{ij}}\left(x_i, X_j\right)$ and, consequently a more accurate computing of the unknown RS profile. Unfortunately such functions are in general related to more complex fitting procedures and, above all, to analytical expressions more complex than polynomials, which can prevent the use of the proposed method by unskilled user; moreover, the lower fitting errors obtained by its use does not allows the user to obtain actually a more accurate calculation of the RS profile, because RS are firstly influenced by unavoidable experimental errors (as positioning errors, machining stresses etc.) that in a generic experimental method of RS analysis (as HDM or similar) lead to a RS uncertainty not less than 10–15 %.

Experimental Analysis

In order to assess the accuracy of the proposed method, it was applied to determine the circumferential RS distribution in aluminium specimens with cold expanded holes by using different degrees of expansion. In more detail, the experimental tests were performed by using 9 specimens of aluminium type 5083 H321 (Fig. 8), whose mechanical properties (Young's modulus E=68.5 GPa, yield stress σ_y=249 MPa and ultimate stress σ_u=351 MPa) were determined by tensile tests. On each specimen holes with nominal diameter d=5.75 mm (see Fig. 8) were drilled. The successive cold expansion was carried out by using three different high-strength steel conical-cylindrical pins (yield stress σ_y=660 MPa, failure stress σ_f=830 MPa), whose diameter D determines a percentage interferences equal to 4 %, 8 % and 10 % respectively.

Before forcing the hole, the pin surface was oiled to reduce the friction between the contact surfaces. The forcing load has been applied by using a materials testing machine with a speed equal to 2 mm/min.

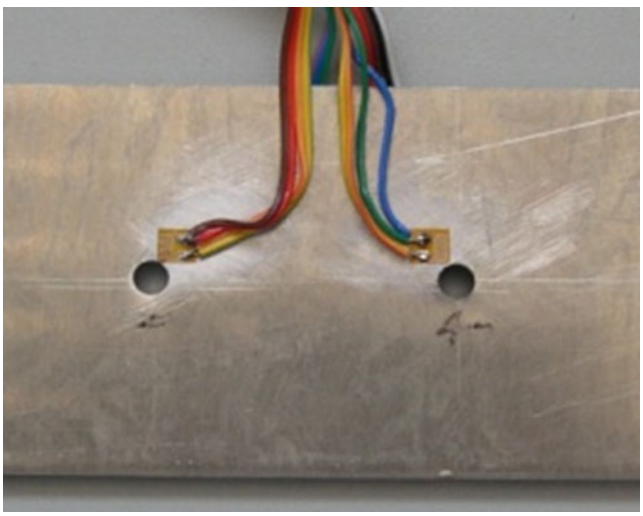

Fig. 8 Particular of strain gauge installation on the specimens used in the test

After forcing, each specimen was instrumented by two MM SGs type CEA-13-060CP-120 (see Fig. 8) with d_1= 0.3 mm and d_2=0 mm.

The device used to mill the grooves is a special three-axis machine (named RESTAN®) produced by SINT Technology SRL and traded by HBM (see Fig. 9(a)). It has a mobile unit equipped with an optical microscope that allows the user to obtain a precise tool positioning, a high-speed (300000 rpm) air turbine with a small tungsten-carbide mill (diameter 1.8 mm) that allows to minimize the residual stresses introduced by machining. The device is also equipped by an electric contact that permits an accurate positioning of the mill on the work surface of metallic components. All the three grooves have been machined by 10 successive feeds with increasing amplitude in order to obtain a better definition of the relaxed strain curves near the hole edge.

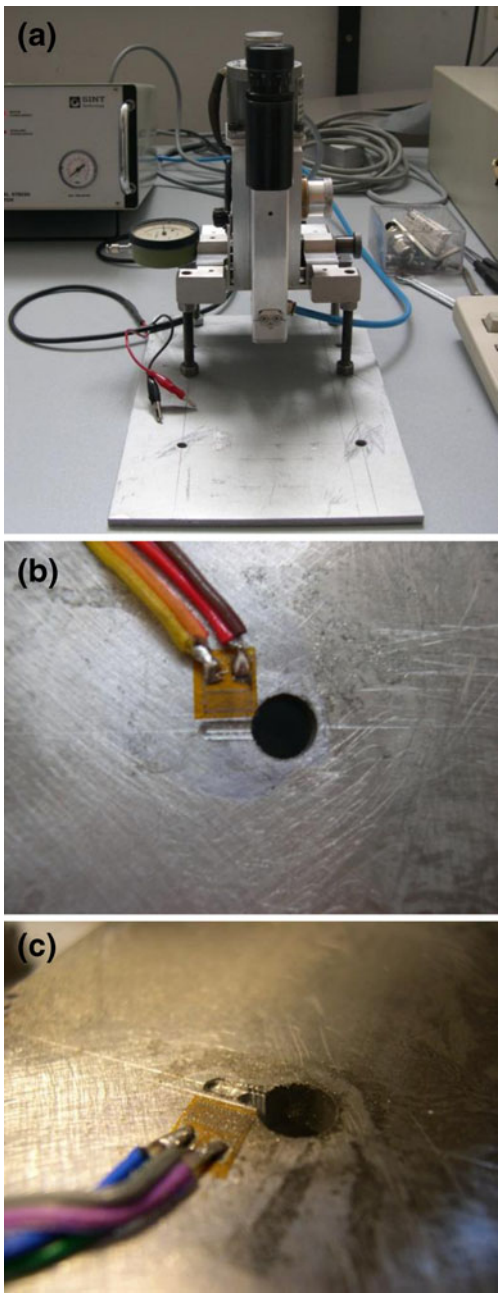

Fig. 9 (**a**) special three-axis machine used to mill the grooves, (**b**) image of groove 1 completed and (**c**) image of groove 3 with 3 feeds executed

Figure 9(b) and (c) show two images of the grooves with different feeds; in detail, Fig. 9(b) shows the first groove completed after 10 feeds, Fig. 9(c) shows the third groove with seven feeds performed.

As an example, Fig. 10 shows the relaxed strains $(\overline{\varepsilon_1}, \overline{\varepsilon_2}, \overline{\varepsilon_3})$ measured by the two SGs after the execution of each feed of the three grooves in case of a hole with degree of expansion 4 %; the experimental strains have been fitted by proper algebraic polynomials to smooth the experimental strain random errors.

After the evaluation of the $\mathbf{C_{ij}}$ matrices (i,j=1,2,3) performed by using the cumulative functions reported in section 4, the unknown circumferential RS were computed from the experimental strains $(\overline{\varepsilon_1}, \overline{\varepsilon_2}, \overline{\varepsilon_3})$ by inverting equation 16. In details, Figs. 11, 12 and 13 show the curves of the so obtained circumferential RS, for the three degrees of expansion considered. Each figure shows the RS profiles relative to three different specimen having the same degrees of expansion; in order to detect the influence of the number of stress positions used in the stress evaluation, it has been varied from 6 to 8 by passing from the first to the third specimen. Figures 11, 12 and 13 show a good repeatability of the results in this stress position range, for each degree of expansion.

In accordance with the theoretical stress predictions (Fig. 1), the results obtained by using the proposed method, show that the region close to the hole edge is subjected to negative circumferential RS that decrease progressively until radial distance of about one half the hole diameter, then they increase and reach positive values at a radial distance of about the hole diameter. In particular, for any stress profile the absolute minimum caused by the phenomenon of *reverse yielding*, widely studied theoretically in [12] and

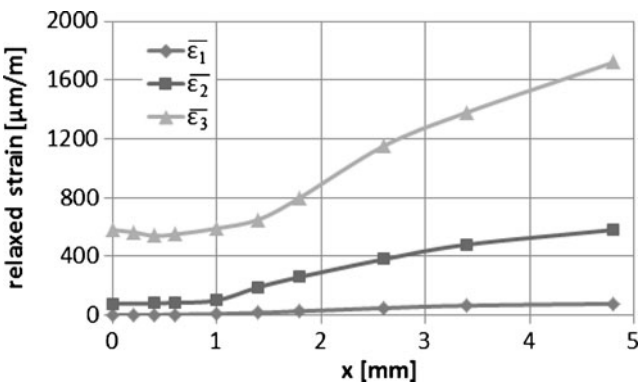

Fig. 10 Plot of the relaxed strains for a hole with degree of expansion 4 %

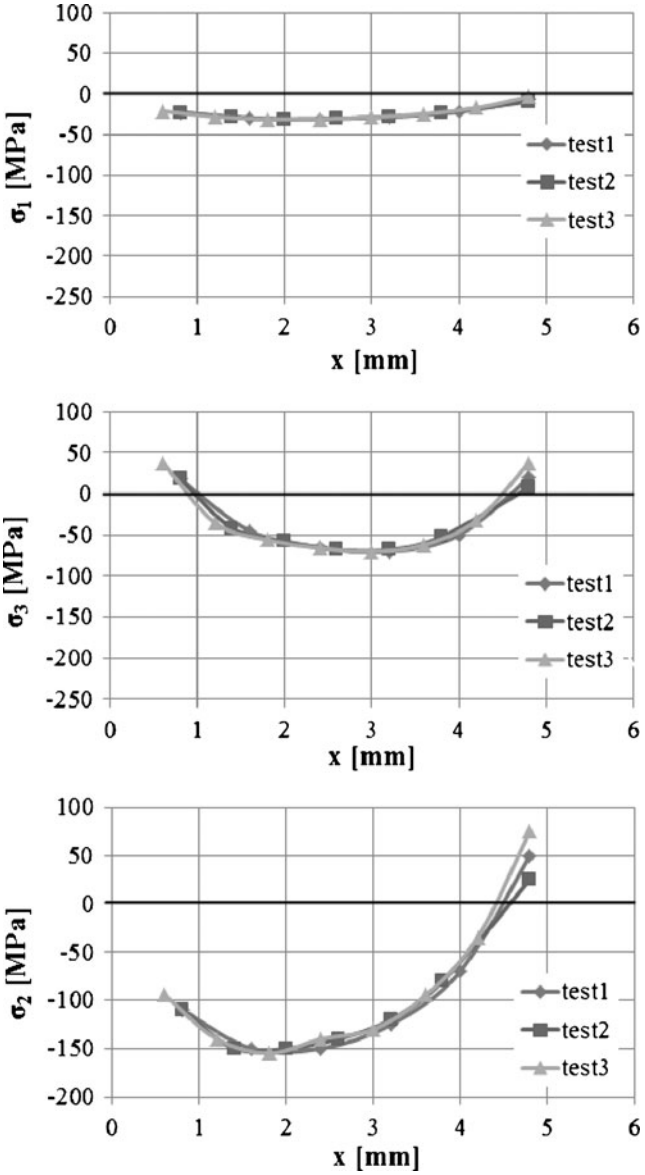

Fig. 11 Plot of the circumferential residual stresses obtained for cold expansion holes with degree of expansion 4 %

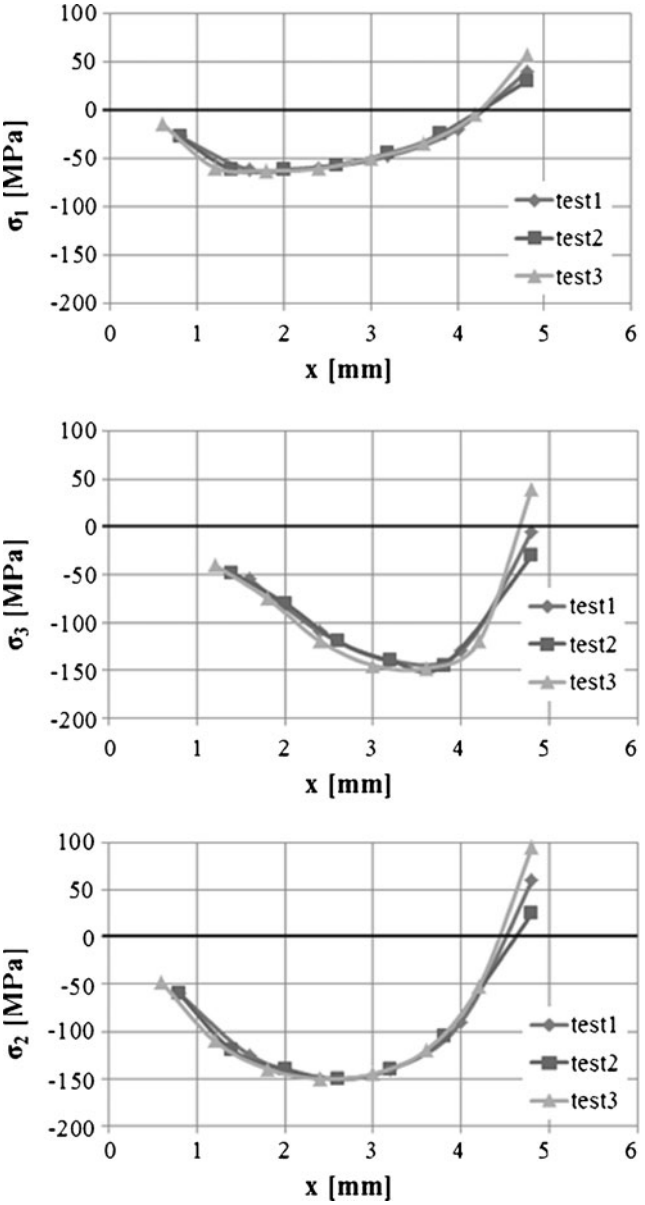

Fig. 12 Plot of the circumferential residual stresses obtained for cold expansion holes with degree of expansion 8 %

experimentally tested in [20, 21], is located at a distance from the hole edge included between 1.5 mm and 3.5 mm; also, the higher values are always taken at the outlet face. For degree of expansion that varies from 4 % to 10 %, such an absolute minimum are in the range 150–225 MPa, i.e in the range 60–90 % of the yield stress.

It is important to note that the proposed method provides an accurate description of the variations of the circumferential RS withy depth, i.e. through the component thickness. In particular, although qualitatively similar circumferential RS distributions are obtained for different degrees of expansion, by moving from the inlet surface toward the outlet surface the absolute minimum value increases significantly. Such a result is in a good agreement with what reported in [21].

Regarding the relationship between the degree of expansion and the fatigue strength, the experimental results provided by the proposed method show that the variations of the circumferential RS with the degree of expansion are negligible in both the outlet face and the middle plane of the component; on the contrary, in the inlet face such variations are significant (minimum value ranging from about 30 MPa for degree of expansion 4 %, to about 80 MPa for degree of expansion 10 %—see Figs. 11, 12 and 13). Consequently, taking into account that the fatigue crack originates always from the hole edge corresponding to the inlet face where the lower compression RS is introduced by HCE, these results explain why the fatigue strength increases with

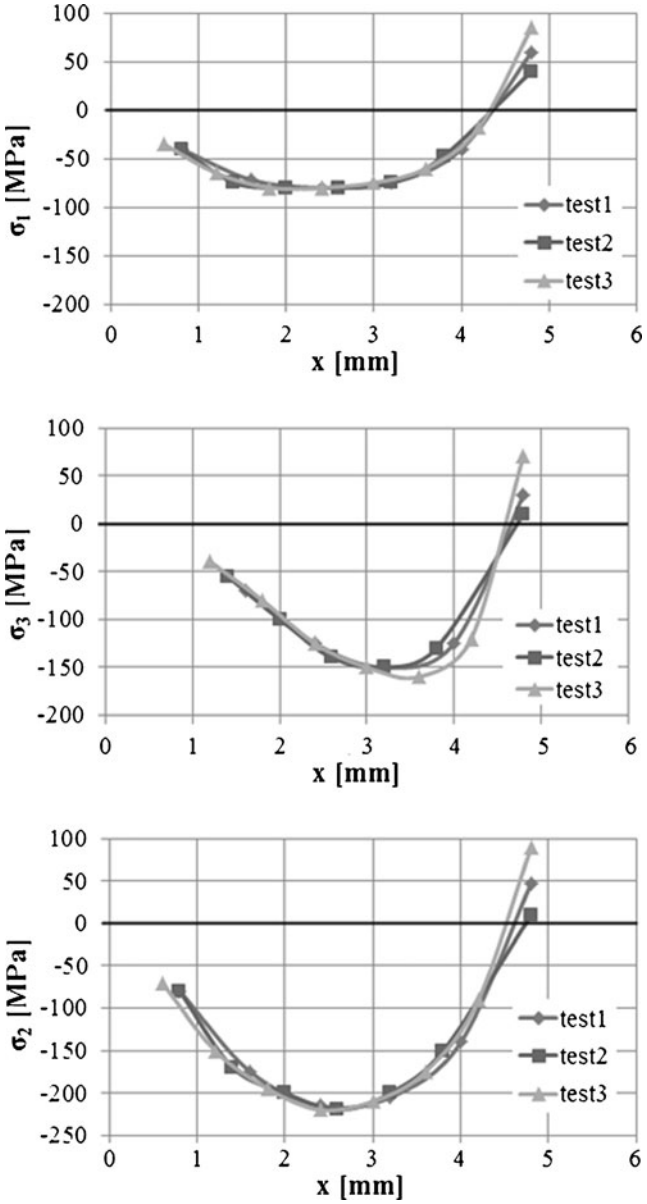

Fig. 13 Plot of the circumferential residual stresses obtained for cold expansion holes with degree of expansion 10 %

the degree of expansion. This is in accordance with the numerical results and the experimental evidence reported in literature [4–6].

Moreover, it is important to observe that for any degree of expansion in the inlet surface the RS are always lower than those measured in the outlet surface; such a result confirms the numerical findings [8], i.e. that for a fixed degree of expansion the higher fatigue strength of the component can be obtained by a double cold expansion of the hole, with the second expansion in the opposite direction to the first one.

To obtain an independent validation of the proposed method, the proposed procedures has been applied to detect the circumferential RS in an aluminium disk having a diameter of 50 mm, that has been externally forced by shrink fit (see Fig. 14(a)). The actual external forcing pressure p_f=1 28,4 MPa has been computed by using the HDM, i.e by drilling a hole having diameter d=6 mm at the centre of the forced disk. After the application the HDM the proposed method has been applied to detect the circumferential RS near the hole. In Fig. 14(b) the circumferential RS profiles provided by the proposed method for the three grooves are compared with the expected profile computed by using the p_f value provided by the HDM and the classical stress formulas of shrink fits [37]. It is seen how the proposed method provide accurate results with errors in general less than 10–12 %.

Such application confirms that the proposed method can be also used for the circumferential RS analysis in a generic component with holes; in fact, the proposed method has been already used for the analysis of the RS close to the holes of flywheels of diesel engines, not subjected to HCE.

Conclusions

The present work proposes a mechanical hybrid numerical-experimental method for the analysis of axial-symmetrical

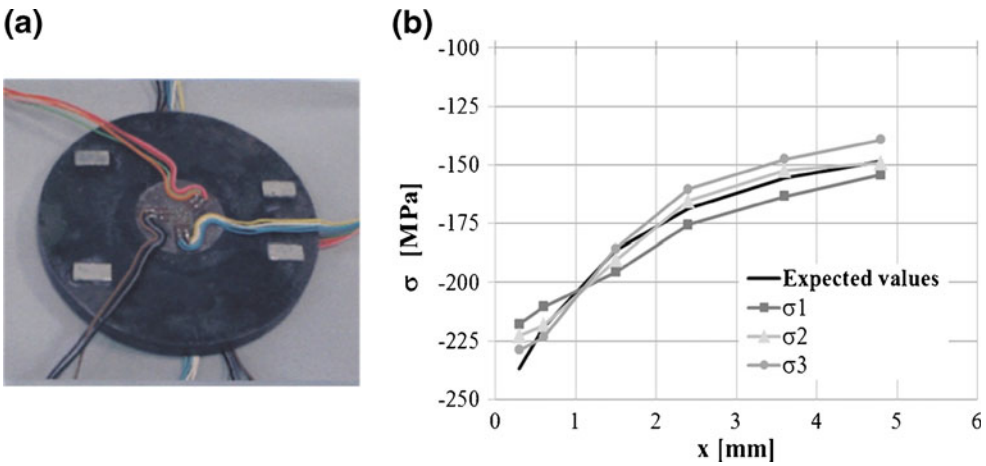

Fig. 14 Independent validation of the proposed method by using a disk subject to an external forcing (**a**): circumferential RS provided by the proposed method and the expected values computed from HDM results (**b**)

residual stresses near holes subjected to cold expansion. The proposed method consist of the execution of three successive radial grooves and the subsequent measurement of the relaxed strains by using two electrical SGs installed on the two opposite surfaces of the component. From the measured strains, the unknown circumferential residual stress distribution can be computed by using an original mathematical formulation that extends the well known Integral Method, and the relative influence coefficients, to the two-dimensional case.

After identifying the geometrical parameters on which the influence coefficients depend (grooves size, depth of successive feeds and SG position), numerical simulations were performed by using the Boundary Element Method to calculate the values of the influence functions for different geometric configurations of the system groove-strain gauge. Such influence functions allow the user to apply the method for any value of actual radial feeds.

The method was applied to the analysis of the circumferential residual stresses close to cold expanded holes in aluminum specimens. In order to characterize the relationship between the degree of expansion and the corresponding circumferential residual stresses, three different degree of expansion were considered. The results obtained agree well with those reported in the literature, showing how the circumferential residual stress distribution introduced by the cold expansion near the hole edge, can be subjected to significant changes with thickness. In particular, at the inlet face the circumferential stresses are relatively small (values ranging between 16 % and 32 % of σ_{yield} for degree of expansion varying from 4 % to 10 %), whereas the higher values are in the outlet face (values ranging between 60 % and 90 % of σ_{yield} for degree of expansion varying from 4 % to 10 %). Consequently, the results obtained by the proposed method confirm the literature evidence that show how in a cold expanded hole fatigue cracks develop (from the hole edge) always in the inlet face where the RS are lower. In addition, the results confirm that fatigue strength increases with increasing degree of expansion.

Finally, in accordance with the results reported in the literature [8], the comparison of the RS in the inlet (from 16 % to 32 % the yield stress) and in the outlet surface (from 60 % to 90 % the yield stress) for various degree of expansion, shows that the higher values of the surface circumferential residual stresses (determining the fatigue strength) can be obtained by using a double cold expansion of the hole, with the second expansion in the opposite direction to the first one, as opposed to using high degrees of expansion.

An independent validation performed by using an aluminium disk externally forced by shrink fit and the well known HDM, has shown that the proposed method provide sufficient accurate results with errors in general less than 10–12 %.

Such an application confirm that, although the method was developed for the analysis of the residual stresses introduced by cold expansion, it can be used to the analysis of the circumferential residual stresses close to a generic hole.

References

1. Champoux RL (1986) Fatigue prevention and design. In: Barnby JT (ed). Camelot Press, London
2. FTI PROCESS SPECIFICATION 8101D (2002) Cold expansion of holes using the standard split sleeve system and countersink cold expansion™ (CsCx™). Engineering Process specification, Fatigue Technology Incorporated Inc., Seattle, Washington
3. Özdemir AT, Edwards L (1996) Measurement of the three-dimensional residual stress distribution around split-sleeve cold-expanded holes. J Strain Anal 31(6):413–421
4. Stefanescu D (2004) Measurement and prediction of fatigue crack growth from cold expanded holes. Part 2: prediction of fatigue crack growth from cold expanded holes. J Strain Anal 39:41–53
5. SohelRana M, Makabe C, Fujiwara G (2009) The effect of hole shape on the extent of fatigue life improvement by cold expansions. Eng Fail Anal 16:2081–2090
6. Gopalakrishna HD, Narasimha Murthy HN, Krishna M, Vinod MS, Suresh AV (2010) Cold expansion of holes and resulting fatigue life enhancement and residual stresses in Al 2024T3 alloy —An experimental study. Eng Fail Anal 17:361–368
7. Backman D, Cowal C, Patterson EA (2010) Analysis of the effects of cold expansion of holes using thermoelasticity and image correlation. Fatig Fract Eng Mater Struct 33(12):859–870
8. Su M, Amrouche A, Mesmacque G, Benseddiq N (2008) Numerical study of double cold expansion of the hole at crack tip and the influence on the residual stress field. Comput Mater Sci 41 (3):350–355
9. Nadai A (1943) Theory of the expanding of boiler and condenser tube joints through rolling. Trans ASME 65:865–880
10. Rich DL, Impellizzeri LF (1977) Fatigue analysis of cold-worked and interference fit fasteners holes. Cyclic Stress Strain and Plastic Deformation Aspects of Fatigue Crack Growth, ASTM STP 637:153–175
11. Guo W (1993) Elastic-plastic analysis of a finite sheet with a cold worked hole. Eng Fract Mech 45:857–864
12. Zhang Y, Fitzpatrick ME, Edwards L (2005) Analysis of the residual stress around a cold-expanded fastener hole in a finite plate. Strain 41:59–70
13. Pavier MJ, Poussard CGC, Smith DJ (1999) Effect of residual stress around cold worked holes on fracture under superimposed mechanical load. Eng Fract Mech 63:751–773
14. Chakherlou TN, Vogwell J (2004) A novel method of cold expansion which creates near uniform compressive tangential residual stress around a fastener hole. Fatig Fract Eng Mater Struct 27:343–351
15. MahendraBabu NC, Jagadish T, Ramachandra K, Sridhara SN (2008) A simplified 3-D finite element simulation of cold expansion of a circular hole to capture through thickness variation of residual stresses. Eng Fail Anal 15(4):339–348
16. Yongshou L, Xiaojun S, Jun L, YueZhufeng (2010) Finite element method and experimental investigation on the residual stress fields and fatigue performance of cold expansion hole. Mater Des 31 (3):1208–1215
17. Stacey A, Macgllivary HJ, Webster GA, Webster PJ, Ziebeck KRA (1985) Measurement of residual by neutron diffraction. J Strain Anal 20(2):93–100

18. Özdemir AT, Wang DQ, Edwards L (1994) Measurement of the 3D residual stress distribution at split sleeve cold expanded holes. Proc. 4th European Conference on Residual Stresses, ICRS-4, Society for Experimental Mechanics Publications 1144–1149
19. Edwards L, Wang DQ (1998) Neutron diffraction determination of the complete 3D residual stress distribution surrounding a cold expanded hole. Proc. 4th European Conference on Residual Stresses. In: Denis S (ed) SociétéFrancaise de Métallurgie et de Matériaux, Bourgogne, France, 2: 619–626
20. Stefanescu D (2004) Measurement and prediction of fatigue crack growth from cold expanded holes. Part 1: the effect of fatigue crack growth on cold expansion residual stresses. J Strain Anal 39:25–40
21. Özdemir AT, Edwards L (2004) Through-thickness residual stress distribution after the cold expansion of fastener holes and its effects on fracturing. J Eng Mater Technol 126:129–135
22. Costanzo F (2005) Analisi delle tensioni residue nei fori espansi a freddo. Master of Science Thesis. University of Palermo, Department of Mechanics
23. Schajer GS, An Y (2010) Residual stress determination using cross-slitting and dual-axis ESPI. Exp Mech 50:169–177
24. Montay G, Sicot O, Maras A, Rouhaud E, Francois M (2009) Two dimensions residual stresses analysis through incremental groove machining with electronic speckle pattern interferometry. Exp Mech 49:459–469
25. Ajovalasit A (1979) Measurement of residual stresses by the hole-drilling method: influence of hole eccentricity. J Strain Anal 14 (4):171–178
26. Petrucci G, Zuccarello B (1997) Modification of the rectilinear groove method for the analysis of uniform residual stresses. Exp Tech 21(6):25–29
27. Ajovalasit A, Petrucci G, Zuccarello B (1996) Determination of nonuniform residual stresses using the ring-core method. J Eng Mater Tech-Trans ASME 118(2):224–229
28. Prime MB (1999) Residual stress measurement by successive extension of a slot: the crack compliance method. Appl Mech Rev 52(2):75–96
29. Vangi D, Tellini S (2010) Hole-drilling strain-gauge method: residual stress measurement with plasticity effects. J Eng Mater Tech, Trans ASME 132(1):11003–11010
30. Beghini M, Bertini L (1998) Recent advances in the hole drilling method for residual stress measurement. J Mater Eng Perform 7 (2):163–173
31. Schajer GS (1988) Measurement of non-uniform residual stresses using the hole-drilling method. Part 1: stress calculation procedures. Trans ASME 110:338–343
32. Schajer GS (1988) Measurement of non-uniform residual stresses using the hole-drilling method. Part 2: practical application of the integral method. Trans ASME 110:344–349
33. Perry CC, Lissner HR (1962) The strain gage primer, ed. Mc Graw-Hill, New York
34. ASTM E 837-99 Standard test method for determining residual stresses by the hole-drilling strain-gage method. ASTM Standard Book, American Society for Testing and Materials, 1916 Race Street, Philadelphia Pennsylvania, 19103 USA.
35. Schajer GS (1981) Application of finite element calculations to residual stress measurement. J Eng Mater Technol 103(2):157–163
36. Zuccarello B (1999) Optimal calculation steps for the evaluation of residual stress by the incremental hole-drilling method. Exp Mech 39(2):117–124
37. Shigley JS, Mische RC (2001) Mechanical engineering design. McGraw Hill